Asociación Argentina
de Mecánica Computacional

Mecánica Computacional Vol XXIX, págs. 449-472 (artículo completo)
Eduardo Dvorkin, Marcela Goldschmit, Mario Storti (Eds.)
Buenos Aires, Argentina, 15-18 Noviembre 2010

MESHLESS APPROXIMATION OF INITIALLY CURVED SHELLS: LINEAR MODEL

Jorge C. Costa[a], Carlos M. Tiago[b], Paulo de M. Pimenta[a] and Eduardo M. B. Campello[a]

[a]*Laboratório de Mecânica Computacional, Escola Politécnica da Universidade de São Paulo, P.O. Box 61548, 05424-970, São Paulo, SP, Brasil,* [*jorgecosta,ppimenta,campello*]*@usp.br*

[b]*Instituto Superior Técnico, Universidade Técnica de Lisboa, Av. Rovisco Pais, 1049-001, Lisboa, Portugal, carlos.tiago@civil.ist.utl.pt*

Keywords: Shells, Meshless Methods, Consistent Linearization.

Abstract. This work develops a kinematically linear shell model departing from a consistent nonlinear theory. Starting with a flat reference configuration for the shell midsurface, an initial (curved) geometry is imposed as a stress-free deformation, after which, the actual motion of the shell takes place. This strategy leads to the use of only orthogonal frames, precluding the use of objects as Christoffel symbols, the second fundamental form or 3-D degenerated solids. The resort to a flat reference configuration allows the use of 2-D Moving Least Squares approximations. The resulting model inherits the same features of the original formulation in the sense that (i) cross-sectional stresses and strains are defined in a totally consistent way, rendering a complete stress-resultant theory and (ii) first order shear deformations are accounted for, as Reissner-Mindlin kinematics is assumed, based on an inextensible director (no thickness changes). A variational statement of the shell model is presented, where the domain displacements and kinematic boundary reactions are independently approximated, hence falling in the category of the hybrid displacement formulations. The discretization of this variational form is made using the Multiple Fixed Least-Squares (MFLS) approximation on the domain and simple Lagrange polynomials on the boundary. The presented model is assessed through several numerical examples and results are compared to those in the literature. The smoothness and convergence of the meshless approximation is discussed. The present scheme's use of only orthogonal frames, along with the consistent definition of stress resultants and consequent plane stress definition led to a neat, consistent formulation for the analysis of initially curved shells. The consistent linear approximation, combined with MFLS approximation, lead to fast computations with high continuity, thus, smooth results for the displacement, strain and stress fields.

1 INTRODUCTION

For about half a century, the Finite Element Method have been developed and improved, becoming the standard approximation method in most numerical simulations. Its limitations are now, due to the devotion of many researchers, largely known and, as far as possible, overcome.

However, some difficulties endure, as lack of precision with large mesh distortions, the need of a fine mesh for high gradient problems, loss of homogeneity and isotropy due to mesh orientation and, most important, difficulties on obtaining a high order of approximation.

This deficiency led to the research of approximation methods that could provide a higher order of continuity to the results, such as the Meshless Methods. According to Li and Liu (2004), "It can easily provide a smooth higher order interpolation field in any dimension, which makes the implementation of both single primary variable Galerkin variational formulations and mixed Galerkin variational formulations easy".

The present work uses some of those advantages in the study of shells. It uses the shell theory developed by Pimenta and Campello (2009) approximating the trial and test spaces by Moving Least Squares (MLS) as in Tiago (2007). It is a particularization of the latter, as the displacements and rotations are taken to be small.

The shell theory therein follows the effort dedicated to developing consistent geometrically exact formulations of beams and shell structural theories made by Simo (1985); Pimenta (1993); Simo *et al.* (1989), their subsequent FEM implementation by Pimenta and Yojo (1993) and Campello, Pimenta and Wriggers (2004) and meshless discretization by Tiago and Pimenta (2005) and (2008), and the considerations of initially deformed structures as in Pimenta (1996) and Pimenta and Campello (2009).

The latest work presents the summation of this effort as a shell theory that departs from a flat reference configuration, from which the initial configuration is mapped as a stress-free deformation. From this initial curved configuration the actual motion takes place. This strategy precludes the use of metrics of differential geometry as it only uses orthogonal frames. It also dismisses some objects as Christoffel Symbols. Another important characteristic is that it isn't based on degenerated solids, but on kinematical impositions, rendering a theory in which "(i) cross-sectional stresses and strains are defined in a totally consistent way, rendering a complete stress-resultant theory, (ii) first-order shear deformations are accounted for, as Reissner–Mindlin kinematics is assumed based on an inextensible director (no thickness changes)" (Pimenta and Campello, 2009).

The generalized effective strains are then taken in their first order (linear in the displacements and rotations). A linear material is also adopted to relate the effective stresses and strains. Assessment is made to the integration over the shell thickness.

Throughout the text, italic Greek or Latin lowercase letters $(a, b, \ldots, \alpha, \beta, \ldots)$ denote scalar quantities, bold italic Greek or Latin lowercase letters $(\boldsymbol{a}, \boldsymbol{b}, \ldots, \boldsymbol{\alpha}, \boldsymbol{\beta}, \ldots)$ denote vectors and bold italic Greek or Latin capital letters $(\boldsymbol{A}, \boldsymbol{B}, \ldots)$ denote second-order tensors in a three-dimensional Euclidean space. Summation convention over repeated indices is adopted, with Greek indices ranging from 1 to 2 and Latin indices from 1 to 3.

2 MESHLESS APPROXIMATION

2.1 Moving Least Squares

Let u be a function on the domain Ω. The approximation u^h of this function around a point $\boldsymbol{x} \in \Omega$ may be expressed by a linear combination of a set of functions named basis, as in

$$u^h(\boldsymbol{x}) = \boldsymbol{p}(\boldsymbol{x}) \cdot \boldsymbol{a}(\boldsymbol{x}), \tag{1}$$

where $\boldsymbol{p}(\boldsymbol{x})$ gathers the basis and $\boldsymbol{a}(\boldsymbol{x})$ the coefficients for the linear combination. If a set of particles (defined positions in the domain Ω) $\overline{\boldsymbol{x}}$ are associated to a set of nodal values $\overline{\boldsymbol{u}}$, the approximation in those nodes can be gathered in

$$\boldsymbol{u}^h = \boldsymbol{P}\boldsymbol{a}\left(\boldsymbol{x}\right), \tag{2}$$

being each column of $\boldsymbol{P}$ the basis evaluated at each point of $\overline{\boldsymbol{x}}$. The coeficients $\boldsymbol{a}\left(\boldsymbol{x}\right)$ can be obtained through the minimization of the weighted error

$$J(\boldsymbol{a}) = \sum_{i=1}^{n} w\left(\boldsymbol{x} - \overline{\boldsymbol{x}}_i\right)\left(\overline{u}_i - u^h\left(\overline{\boldsymbol{x}}_i\right)\right)^2 \tag{3}$$

with respect to $\boldsymbol{a}$. In (3), $w\left(\boldsymbol{x} - \overline{\boldsymbol{x}}_i\right)$ is a weighting function that enforces the local character of the approximation. Discursion on the properties of this function can be found along with examples in Tiago (2007). This minimization renders the linear sytem of equations

$$\boldsymbol{A}^x\boldsymbol{a}^x = \boldsymbol{B}^x\overline{\boldsymbol{u}}, \tag{4}$$

where

$$\begin{aligned} \boldsymbol{A}^x &= \sum_{i=1}^{n} w\left(\boldsymbol{x} - \overline{\boldsymbol{x}}_i\right)\boldsymbol{A}_i \\ \boldsymbol{A}_i &= \boldsymbol{p}\left(\overline{\boldsymbol{x}}_i\right)\boldsymbol{p}\left(\overline{\boldsymbol{x}}_i\right)^T \\ \boldsymbol{B}^x &= \left[w\left(\boldsymbol{x} - \overline{\boldsymbol{x}}_1\right)\boldsymbol{p}\left(\overline{\boldsymbol{x}}_1\right) \quad w\left(\boldsymbol{x} - \overline{\boldsymbol{x}}_2\right)\boldsymbol{p}\left(\overline{\boldsymbol{x}}_2\right) \quad \cdots \quad w\left(\boldsymbol{x} - \overline{\boldsymbol{x}}_n\right)\boldsymbol{p}\left(\overline{\boldsymbol{x}}_n\right)\right] \end{aligned}. \tag{5}$$

The approximation can then be expressed as

$$u^h\left(\boldsymbol{x}\right) = \boldsymbol{p}\left(\boldsymbol{x}\right)\boldsymbol{A}^{-1}\left(\boldsymbol{x}\right)\boldsymbol{B}\left(\boldsymbol{x}\right)\overline{\boldsymbol{u}}, \tag{6}$$

or, resorting to the shape functions $\Phi_i\left(\boldsymbol{x}\right)$, as

$$u^h\left(\boldsymbol{x}\right) = \sum_{i=1}^{n} \Phi_i\left(\boldsymbol{x}\right)\overline{u}_i, \tag{7}$$

being

$$\Phi_i\left(\boldsymbol{x}\right) = \boldsymbol{p}\left(\boldsymbol{x}\right)\boldsymbol{A}^{-1}\left(\boldsymbol{x}\right)\boldsymbol{B}_i\left(\boldsymbol{x}\right), \tag{8}$$

and $\boldsymbol{B}_i\left(\boldsymbol{x}\right)$ the i^{th} column of $\boldsymbol{B}$. The shape functions can be gathered in the vector $\boldsymbol{\Phi}$, so the approximation and its derivatives can be expressed by

$$\begin{aligned} u^h\left(\boldsymbol{x}\right) &= \boldsymbol{\Phi}\left(\boldsymbol{x}\right)\overline{\boldsymbol{u}} \\ u^h{}_{,i}\left(\boldsymbol{x}\right) &= \boldsymbol{\Phi}_{,i}\left(\boldsymbol{x}\right)\overline{\boldsymbol{u}} \end{aligned}. \tag{9}$$

The derivative of the shape functions can easily be obtained directly from (8) and expressed by

$$\boldsymbol{\Phi}_{,i}\left(\boldsymbol{x}\right) = \boldsymbol{p}_{,i}\boldsymbol{A}^{-1}\boldsymbol{B} + \boldsymbol{p}\left[\boldsymbol{A}^{-1}\right]_{,i}\boldsymbol{B} + \boldsymbol{p}\boldsymbol{A}^{-1}\boldsymbol{B}_{,i}, \tag{10}$$

as the derivative of the moment matrix is taken as

$$\left[\boldsymbol{A}^{-1}\right]_{,i} = -\boldsymbol{A}^{-1}\boldsymbol{A}_{,i}\boldsymbol{A}^{-1}, \tag{11}$$

2.2 Multiple Fixed Least Squares

The definition of a weighting function in the whole domain can be a burdensome task. The common practice when dealing with Moving Least Squares is to define the weight on the particles $\bar{x}$ rather than in the interest points x. This fact was pointed out by Tiago (2007) where the approximation defined in this way is called Multiple Fixed Least Squares (MFLS).

Although this seems as a minor theoretical difference, it has major implementation repercussions. Throughout this text and in most of the implementations found in the literature, the shape function is the same in the whole domain, but the parameter that defines its support varies. In this case, the difference between MLS and MFLS is that, instead of storing these parameters for every interest point, it's associated with each particle in the distribution. The approximation, the shape function and its derivatives are the same as defined in the previous section.

Some observations concerning the approximation in this work must also be made. The support of the cloud associated to each particle is defined as to, in every interest point (e.g. integration quadrature sample point, load application point), the approximation can be defined (the moment matrix can be inverted). The used weight function is the adjustable spline of order 3.

$$w\left(r\right) = \begin{cases} \left(1 - r^2\right)^3, \text{ if } r \leq 1 \\ 0, \text{ if } r > 1 \end{cases}, \tag{12}$$

3 NONLINEAR SHELLS

3.1 Introduction

This chapter presents the shell theory described in Pimenta and Campello (2009) for shells encompassing finite displacements and rotations. For now, no assumption is made concerning the magnitude of such quantities; only in the next chapter the theory is linearized.

The shell is described in a flat reference configuration. The initial curved configuration is then obtained in a stress-free transformation after which the actual or effective transformation takes place.

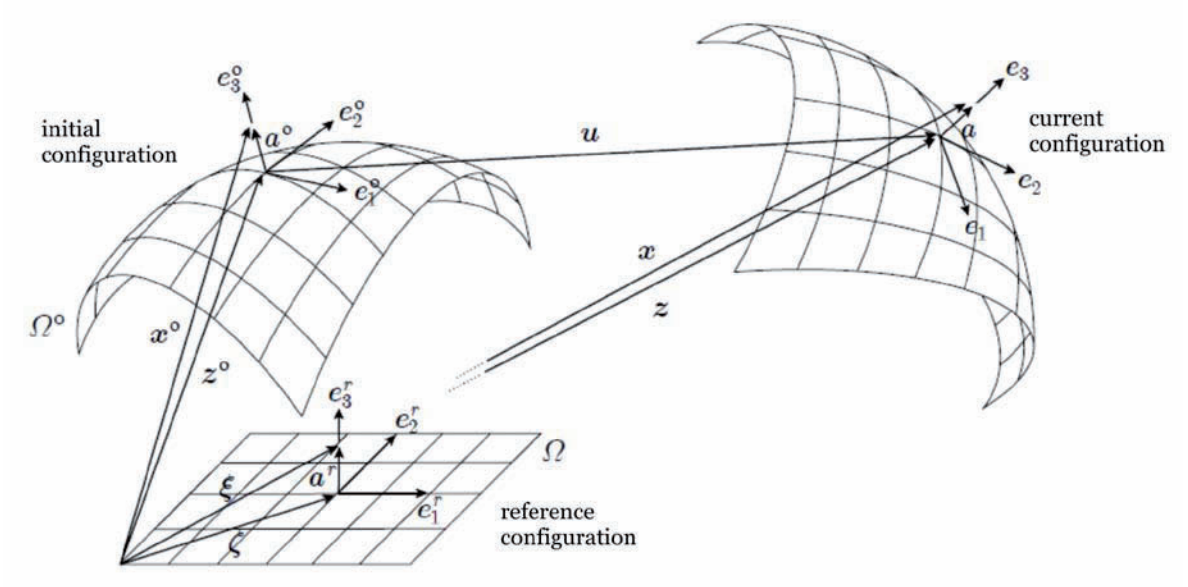

Figure 1: Shell kinematics

All the back-rotated quantities and integrations are defined in the flat reference surface Ω^r, referred to as the shell midsurface (although it may not actually be in the middle of the shell's thickness). Let $\boldsymbol{e}_i^r$ be a orthogonal frame where $\boldsymbol{e}_\alpha^r$ are aligned to the midsurface and $\boldsymbol{e}_3^r$ is orthogonal to them.

In Ω^r, a point in the shell can be described by its position

$$\boldsymbol{\xi} = \boldsymbol{\zeta} + \boldsymbol{a}^r \tag{13}$$

where $\boldsymbol{\zeta} = \xi_\alpha \boldsymbol{e}_\alpha$ defines the projection of this position in the midsurface and $\boldsymbol{a}^r = \xi_3 \boldsymbol{e}_3^r$ is the through-the-thickness component. The triad $\left\{\xi_1, \xi_2, \xi_3\right\}$ defines a Cartesian system in three dimensions.

3.2 Kinematics

The initial deformation is a mapping from the flat reference to the initial configuration. The displacement of the shell midsurface points are described as

$$\boldsymbol{z}^o = \boldsymbol{z}^o\left(\xi_\alpha\right). \tag{14}$$

This deformation is assumed to be of Kirchhoff-Love type. The director $\boldsymbol{a}^o$ is then perpendicular to the shell curvature. The frame $\boldsymbol{e}_i^o$, that follows this director, is obtained from the rotation of the reference director:

$$\begin{aligned} \boldsymbol{a}_i^o &= \boldsymbol{Q}^o \boldsymbol{a}_i^r \\ \boldsymbol{Q}^o &= \boldsymbol{e}_i^o \otimes \boldsymbol{e}_i^r \\ \boldsymbol{e}_1^o = \frac{\boldsymbol{z}_{,1}^o}{\left\|\boldsymbol{z}_{,1}^o\right\|},\ \boldsymbol{e}_3^o &= \frac{\boldsymbol{z}_{,1}^o \times \boldsymbol{z}_{,2}^o}{\left\|\boldsymbol{z}_{,1}^o \times \boldsymbol{z}_{,2}^o\right\|},\ \boldsymbol{e}_2^o = \boldsymbol{e}_3^o \times \boldsymbol{e}_1^o \end{aligned} \quad . \tag{15}$$

The deformation gradient for the initial deformation can be expressed by

$$\begin{aligned} \boldsymbol{F}^o = \frac{\partial \boldsymbol{x}^o}{\partial \boldsymbol{\xi}} &= \left(\boldsymbol{z}_{,\alpha}^o - \boldsymbol{Q}^o \boldsymbol{e}_\alpha^r + \boldsymbol{Q}_{,\alpha}^o \boldsymbol{Q}^{oT} \boldsymbol{a}^o\right) \otimes \boldsymbol{e}_\alpha^r + \boldsymbol{Q}^o \\ &= \left(\boldsymbol{\eta}_\alpha^o + \boldsymbol{K}_\alpha^o \boldsymbol{a}^o\right) \otimes \boldsymbol{e}_\alpha^r + \boldsymbol{Q}^o \end{aligned}, \tag{16}$$

where the generalized membrane strain vectors

$$\boldsymbol{\eta}_\alpha^o = \boldsymbol{z}_{,\alpha}^o - \boldsymbol{Q}^o \boldsymbol{e}_\alpha^r, \tag{17}$$

and the curvature skew-symmetric tensors

$$\boldsymbol{K}_\alpha^o = \boldsymbol{Q}_{,\alpha}^o \boldsymbol{Q}^{oT} = \boldsymbol{e}_{i,\alpha}^o \otimes \boldsymbol{e}_i^o, \tag{18}$$

are defined. The axial vector of $\boldsymbol{K}_\alpha^o$ are

$$\boldsymbol{\kappa}_\alpha^o = \operatorname{axial}\left(\boldsymbol{K}_\alpha^o\right) = \left(\boldsymbol{e}_{2,\alpha}^o \cdot \boldsymbol{e}_3^o\right)\boldsymbol{e}_1^o + \left(\boldsymbol{e}_{3,\alpha}^o \cdot \boldsymbol{e}_1^o\right)\boldsymbol{e}_2^o + \left(\boldsymbol{e}_{1,\alpha}^o \cdot \boldsymbol{e}_2^o\right)\boldsymbol{e}_1^o, \tag{19}$$

and the generalized initial strains can be summoned in the vectors

$$\boldsymbol{\gamma}_\alpha^o = \boldsymbol{\eta}_\alpha^o + \boldsymbol{\kappa}_\alpha^o \times \boldsymbol{a}^o, \tag{20}$$

so the initial deformation gradient can be neatly written as

$$\boldsymbol{F}^o = \boldsymbol{\gamma}_\alpha^o \otimes \boldsymbol{e}_\alpha^r + \boldsymbol{Q}^o, \tag{21}$$

Those quantities are affected by rigid body motions and are not suitable for an objective theory. Therefore, it's compelling to work with their back-rotated counterparts, not affected by such motions:

$$\begin{aligned}
\boldsymbol{\gamma}_{\alpha}^{or} &= \boldsymbol{Q}^{oT}\boldsymbol{\gamma}_{\alpha}^{o} = \boldsymbol{\eta}_{\alpha}^{or} + \boldsymbol{\kappa}_{\alpha}^{or} \times \boldsymbol{a}^{r} \\
\boldsymbol{\eta}_{\alpha}^{or} &= \boldsymbol{Q}^{oT}\boldsymbol{\eta}_{\alpha}^{o} = \boldsymbol{Q}^{oT}\boldsymbol{z}_{,\alpha}^{o} - \boldsymbol{e}_{\alpha}^{r} \\
\boldsymbol{\kappa}_{\alpha}^{or} &= \boldsymbol{Q}^{oT}\boldsymbol{\kappa}_{\alpha}^{o} = \left(\boldsymbol{e}_{2,\alpha}^{o} \cdot \boldsymbol{e}_{3}^{o}\right)\boldsymbol{e}_{1}^{r} + \left(\boldsymbol{e}_{3,\alpha}^{o} \cdot \boldsymbol{e}_{1}^{o}\right)\boldsymbol{e}_{2}^{r} + \left(\boldsymbol{e}_{1,\alpha}^{o} \cdot \boldsymbol{e}_{2}^{o}\right)\boldsymbol{e}_{3}^{r}
\end{aligned} \quad . \tag{22}$$

It's also possible to define a back-rotated deformation gradient such as $\boldsymbol{F}^{o} = \boldsymbol{Q}^{o}\boldsymbol{F}^{or}$

$$\begin{aligned}
\boldsymbol{F}^{or} &= \boldsymbol{f}_{i}^{or} \otimes \boldsymbol{e}_{i}^{r} \\
\boldsymbol{f}_{\alpha}^{or} &= \boldsymbol{e}_{\alpha}^{r} + \boldsymbol{\gamma}_{\alpha}^{or} \\
\boldsymbol{f}_{3}^{or} &= \boldsymbol{e}_{3}^{r}
\end{aligned} . \tag{23}$$

The inverse of this transformation is given by

$$\begin{aligned}
\boldsymbol{F}^{o-1} &= \frac{1}{J^{o}}\left(\boldsymbol{e}_{i}^{r} \otimes \boldsymbol{g}_{i}^{or}\right)\boldsymbol{Q}^{oT} \\
J^{o} &= \det \boldsymbol{F}^{o} = \boldsymbol{e}_{3}^{r} \cdot \boldsymbol{f}_{1}^{or} \times \boldsymbol{f}_{2}^{or} \\
\boldsymbol{g}_{1}^{or} &= \boldsymbol{f}_{2}^{or} \times \boldsymbol{e}_{3}^{r} \\
\boldsymbol{g}_{2}^{or} &= \boldsymbol{e}_{3}^{r} \times \boldsymbol{f}_{1}^{or} \\
\boldsymbol{g}_{3}^{or} &= \boldsymbol{f}_{1}^{or} \times \boldsymbol{f}_{2}^{or}
\end{aligned} \quad . \tag{24}$$

The effective motion of the shell can be described in the same manner. The displacement of the midsurface is $\boldsymbol{u}$ and the rotation of the director is given by $\boldsymbol{Q}^{e} = \boldsymbol{e}_{i} \otimes \boldsymbol{e}_{i}^{o}$. This time, the rotation is independent of the displacement, as Reissner-Mindlin kinematics is assumed. $\boldsymbol{Q}^{e}$ can be described by the Euler parameters grouped in the rotation vector $\boldsymbol{\theta}$ through the Euler-Rodrigues relation:

$$\boldsymbol{Q} = \boldsymbol{I} + h_{1}\left(\theta\right)\boldsymbol{\Theta} + h_{2}\left(\theta\right)\boldsymbol{\Theta}^{2}, \tag{25}$$

where

$$\begin{aligned}
\boldsymbol{\Theta} = \mathrm{Skew}\left(\boldsymbol{\theta}\right) &= \begin{bmatrix} 0 & -\theta_{3} & \theta_{2} \\ \theta_{3} & 0 & -\theta_{1} \\ -\theta_{2} & \theta_{1} & 0 \end{bmatrix}, \\
\theta &= \left\|\boldsymbol{\theta}\right\|, \\
h_{1}\left(\theta\right) &= \frac{\sin\left(\theta\right)}{\theta}, \\
h_{2}\left(\theta\right) &= \frac{1}{2}\left(\frac{\sin\left(\theta/2\right)}{\theta/2}\right)^{2}
\end{aligned} \quad . \tag{26}$$

The final position of a point in the shell can be expressed by

$$\boldsymbol{x} = \boldsymbol{z} + \boldsymbol{a} = \boldsymbol{z}^{o} + \boldsymbol{u} + \boldsymbol{Q}^{e}\boldsymbol{a}^{o} \tag{27}$$

The three components of $\boldsymbol{u}$ along with the three components of $\boldsymbol{\theta}$ in a global Cartesian System define the six degrees of freedom of the theory.

The deformation from the flat reference configuration to the current deformed configuration

is called the total deformation, and its gradient is given by

$$\begin{aligned}\boldsymbol{F} &= \frac{\partial \boldsymbol{x}}{\partial \boldsymbol{\xi}} \\ &= \left(\boldsymbol{z}^{o}_{,\alpha} + \boldsymbol{u}_{,\alpha} - \boldsymbol{e}_{\alpha} + \boldsymbol{Q}_{,\alpha}\boldsymbol{Q}^{T}\boldsymbol{a}\right) \otimes \boldsymbol{e}^{r}_{\alpha} + \boldsymbol{e}_{i} \otimes \boldsymbol{e}^{r}_{i}\,, \\ &= \left(\boldsymbol{\eta}_{\alpha} + \boldsymbol{K}_{\alpha}\boldsymbol{a}\right) \otimes \boldsymbol{e}^{r}_{\alpha} + \boldsymbol{Q}\end{aligned} \tag{28}$$

where, as in (17)-(19), one can define

$$\boldsymbol{\eta}_{\alpha} = \boldsymbol{z}^{o}_{,\alpha} + \boldsymbol{u}_{,\alpha} - \boldsymbol{e}_{\alpha} = \boldsymbol{z}_{,\alpha} - \boldsymbol{Q}\boldsymbol{e}^{r}_{\alpha}, \tag{29}$$

$$\boldsymbol{K}_{\alpha} = \boldsymbol{Q}_{,\alpha}\boldsymbol{Q}^{T} = \boldsymbol{K}^{e}_{\alpha} + \boldsymbol{Q}^{e}\boldsymbol{K}^{o}_{\alpha}\boldsymbol{Q}^{eT}, \tag{30}$$

$$\boldsymbol{\kappa}_{\alpha} = \operatorname{axial}\left(\boldsymbol{K}^{e}_{\alpha} + \boldsymbol{Q}^{e}\boldsymbol{K}^{e}_{\alpha}\boldsymbol{Q}^{eT}\right) = \boldsymbol{\kappa}^{e}_{\alpha} + \boldsymbol{Q}^{e}\boldsymbol{\kappa}^{o}_{\alpha}\text{, and} \tag{31}$$

$$\boldsymbol{\gamma}^{r}_{\alpha} = \boldsymbol{\eta}^{r}_{\alpha} + \boldsymbol{\kappa}^{r}_{\alpha} \times \boldsymbol{a}^{r}, \tag{32}$$

so (28) can be expressed by

$$\boldsymbol{F} = \boldsymbol{Q}\left(\boldsymbol{I} + \boldsymbol{\gamma}^{r}_{\alpha} \otimes \boldsymbol{e}^{r}_{\alpha}\right). \tag{33}$$

As in (23),

$$\begin{aligned}\boldsymbol{F}^{r} &= \boldsymbol{I} + \boldsymbol{\gamma}^{r}_{\alpha} \otimes \boldsymbol{e}^{r}_{\alpha} = \boldsymbol{f}^{r}_{i} \otimes \boldsymbol{e}^{r}_{i} \\ \boldsymbol{f}^{r}_{\alpha} &= \boldsymbol{e}^{r}_{\alpha} + \boldsymbol{\gamma}^{r}_{\alpha} \qquad . \\ \boldsymbol{f}^{r}_{3} &= \boldsymbol{e}^{r}_{3}\end{aligned} \tag{34}$$

The velocity gradient can be obtained by differentiation of (34) in time, rendering

$$\dot{\boldsymbol{F}} = \boldsymbol{\Omega}\boldsymbol{F} + \boldsymbol{Q}\left(\dot{\boldsymbol{\gamma}}^{r}_{\alpha} \otimes \boldsymbol{e}^{r}_{\alpha}\right), \tag{35}$$

where $\boldsymbol{\Omega} = \dot{\boldsymbol{Q}}\boldsymbol{Q}^{T}$ is the spin tensor and

$$\begin{aligned}\dot{\boldsymbol{\gamma}}^{r}_{\alpha} &= \dot{\boldsymbol{\eta}}^{r}_{\alpha} + \dot{\boldsymbol{\kappa}}^{r}_{\alpha} \times \boldsymbol{a}^{r} \\ \dot{\boldsymbol{\eta}}^{r}_{\alpha} &= \boldsymbol{Q}^{T}\left(\dot{\boldsymbol{u}}_{,\alpha} + \boldsymbol{Z}_{,\alpha}\boldsymbol{\Gamma}\dot{\boldsymbol{\theta}}\right) \\ \dot{\boldsymbol{\kappa}}^{r}_{\alpha} &= \boldsymbol{Q}^{T}\left(\boldsymbol{\Gamma}_{,\alpha}\dot{\boldsymbol{\theta}} + \boldsymbol{\Gamma}\dot{\boldsymbol{\theta}}_{,\alpha}\right) \\ \boldsymbol{Z}_{,\alpha} &= \operatorname{Skew}\left(\boldsymbol{z}_{,\alpha}\right) \qquad . \\ \boldsymbol{\Gamma}_{,\alpha} &= h_{2}\left(\theta\right)\boldsymbol{\Theta}_{,\alpha} + h_{3}\left(\theta\right)\left(\boldsymbol{\Theta}\boldsymbol{\Theta}_{,\alpha} + \boldsymbol{\Theta}_{,\alpha}\boldsymbol{\Theta}\right) + \\ &\quad + h_{4}\left(\theta\right)\left(\boldsymbol{\theta}\cdot\boldsymbol{\theta}_{,\alpha}\right)\boldsymbol{\Theta} + h_{5}\left(\theta\right)\left(\boldsymbol{\theta}\cdot\boldsymbol{\theta}_{,\alpha}\right)\boldsymbol{\Theta}^{2} \\ h_{4}\left(\theta\right) &= \frac{h_{1}\left(\theta\right) - 2h_{2}\left(\theta\right)}{\theta^{2}} \quad \text{and} \quad h_{5}\left(\theta\right) = \frac{h_{2}\left(\theta\right) - 3h_{3}\left(\theta\right)}{\theta^{2}}\end{aligned} \tag{36}$$

The total deformation can be decomposed in the initial and effective ones as $\boldsymbol{F} = \boldsymbol{F}^{e}\boldsymbol{F}^{o}$, and with the use of (24),

$$\begin{aligned} \boldsymbol{F}^{e} &= \boldsymbol{F}\boldsymbol{F}^{o-1} = \boldsymbol{Q}\Big(\boldsymbol{f}_i^{er} \otimes \boldsymbol{e}_i^{o}\Big) \\ \boldsymbol{f}_\alpha^{\mathrm{e}r} &= J^{\mathrm{o}-1}\Big(\boldsymbol{e}_\alpha^{r} \cdot \boldsymbol{g}_\beta^{\mathrm{o}r}\Big)\boldsymbol{f}_\beta^{r} \\ \boldsymbol{f}_3^{\mathrm{e}r} &= \boldsymbol{f}_3^{r} = \boldsymbol{e}_3^{r} \end{aligned} \quad . \tag{37}$$

By analogy to (34), the effective back-rotated strains can be defined as

$$\boldsymbol{\gamma}_\alpha^{\mathrm{e}r} = \boldsymbol{f}_\alpha^{\mathrm{e}r} - \boldsymbol{e}_\alpha^{r} = J^{o-1}\Big(\boldsymbol{e}_\alpha^{r} \cdot \boldsymbol{g}_\beta^{\mathrm{o}r}\Big)\Big(\boldsymbol{e}_\beta^{r} + \boldsymbol{\gamma}_\beta^{r}\Big) - \boldsymbol{e}_\alpha^{r} \,. \tag{38}$$

3.3 Statics

The first Piola-Kirchhoff effective tensor is

$$\boldsymbol{P}^{\mathrm{e}} = J^{\mathrm{e}}\boldsymbol{T}\boldsymbol{F}^{\mathrm{e}-T}, \tag{39}$$

where $J^e = \det \boldsymbol{F}^e$ is the Jacobian of the effective deformation and $\boldsymbol{T}$ is the Cauchy stress tensor. Its correspondent for the total deformation is

$$\boldsymbol{P} = J\boldsymbol{T}\boldsymbol{F}^{-T} = J^{\mathrm{o}}J^{e}\boldsymbol{T}\boldsymbol{F}^{\mathrm{e}-T}\boldsymbol{F}^{\mathrm{o}-T} = J^{\mathrm{o}}\boldsymbol{P}^{e}\boldsymbol{F}^{\mathrm{o}-T}. \tag{40}$$

Both those vectors can be expressed in their column vectors as

$$\begin{aligned} \boldsymbol{P}^{\mathrm{e}} &= \boldsymbol{\tau}_i^{\mathrm{e}} \otimes \boldsymbol{e}_i^{\mathrm{o}} = \boldsymbol{Q}\boldsymbol{\tau}_i^{\mathrm{e}r} \otimes \boldsymbol{e}_i^{\mathrm{o}} \\ \boldsymbol{P} &= \boldsymbol{\tau}_i \otimes \boldsymbol{e}_i^{r} = \boldsymbol{Q}\boldsymbol{\tau}_i^{r} \otimes \boldsymbol{e}_i^{r} \end{aligned} \,. \tag{41}$$

Using (24) in (39), one can obtain the relationship between them:

$$\begin{aligned} \boldsymbol{\tau}_\alpha^{r} &= \Big(\boldsymbol{g}_\alpha^{or} \cdot \boldsymbol{e}_\beta^{r}\Big)\boldsymbol{\tau}_\beta^{er} \\ \boldsymbol{\tau}_3^{r} &= \Big(\boldsymbol{g}_\alpha^{or} \cdot \boldsymbol{e}_3^{r}\Big)\boldsymbol{\tau}_3^{er} = \Big(\boldsymbol{f}_1^{or} \cdot \boldsymbol{f}_2^{or} \times \boldsymbol{f}_3^{or}\Big)\boldsymbol{\tau}_3^{er} = J^{o}\boldsymbol{\tau}_3^{er} \end{aligned} \,. \tag{42}$$

The shell internal power per unit volume in the reference configuration is

$$\boldsymbol{P} : \dot{\boldsymbol{F}} = J^{o}\boldsymbol{P}^{\boldsymbol{e}} : \dot{\boldsymbol{F}}^{e}. \tag{43}$$

Developing the left side of (43),

$$\boldsymbol{P} : \dot{\boldsymbol{F}} = \boldsymbol{\tau}_\alpha^{r} \cdot \dot{\boldsymbol{\eta}}_\alpha^{r} + \Big(\boldsymbol{a}^{r} \times \boldsymbol{\tau}_\alpha^{r}\Big) \cdot \dot{\boldsymbol{\kappa}}_\alpha^{r} \,. \tag{44}$$

The same power per unit area of Ω^r is obtained through the integration of (44) in the thickness as

$$\begin{aligned} \int_H \Big(\boldsymbol{P} : \dot{\boldsymbol{F}}\Big) dH &= \int_H \Big(\boldsymbol{\tau}_\alpha^{r}\Big) dH \cdot \dot{\boldsymbol{\eta}}_\alpha^{r} + \int_H \Big(\boldsymbol{a}^{r} \times \boldsymbol{\tau}_\alpha^{r}\Big) dH \cdot \dot{\boldsymbol{\kappa}}_\alpha^{r}, \\ &= \boldsymbol{n}_\alpha^{r} \cdot \dot{\boldsymbol{\eta}}_\alpha^{r} + \boldsymbol{m}_\alpha^{r} \cdot \dot{\boldsymbol{\kappa}}_\alpha^{r} \end{aligned} \tag{45}$$

where the vectors

$$\boldsymbol{n}_\alpha^{r} = \int_H \Big(\boldsymbol{\tau}_\alpha^{r}\Big) dH \quad \text{and} \quad \boldsymbol{m}_\alpha^{r} = \int_H \Big(\boldsymbol{a}^{r} \times \boldsymbol{\tau}_\alpha^{r}\Big) dH \tag{46}$$

are, respectively the back-rotated generalized internal resultants of forces and moments. Combining those in the vectors

$$\boldsymbol{\sigma}_\alpha^{r} = \begin{bmatrix} \boldsymbol{n}_\alpha^{r} \\ \boldsymbol{m}_\alpha^{r} \end{bmatrix}, \tag{47}$$

and the time derivatives of the generalized strains in the vectors

$$\dot{\boldsymbol{\varepsilon}}_{\alpha}^{r} = \begin{bmatrix} \dot{\boldsymbol{\eta}}_{\alpha}^{r} \\ \dot{\boldsymbol{\kappa}}_{\alpha}^{r} \end{bmatrix}, \tag{48}$$

such that

$$\dot{\boldsymbol{\varepsilon}}_{\alpha}^{r} = \boldsymbol{\Psi}_{\alpha}\boldsymbol{\Delta}_{\alpha}\dot{\boldsymbol{d}}, \tag{49}$$

where

$$\boldsymbol{\Psi}_{\alpha} = \begin{bmatrix} \boldsymbol{Q}^{T} & \boldsymbol{O} \\ \boldsymbol{O} & \boldsymbol{Q}^{T} \end{bmatrix} \begin{bmatrix} \boldsymbol{I} & \boldsymbol{O} & \boldsymbol{Z}_{,\alpha}\boldsymbol{\Gamma} \\ \boldsymbol{O} & \boldsymbol{\Gamma} & \boldsymbol{\Gamma}_{,\alpha} \end{bmatrix} \quad \text{and} \quad \boldsymbol{\Delta}_{\alpha} = \begin{bmatrix} \boldsymbol{I}\dfrac{\partial}{\partial\xi_{\alpha}} & \boldsymbol{O} \\ \boldsymbol{O} & \boldsymbol{I}\dfrac{\partial}{\partial\xi_{\alpha}} \\ \boldsymbol{O} & \boldsymbol{I} \end{bmatrix}, \tag{50}$$

(45) can be gathered as

$$\int_{H}\left(\boldsymbol{P} : \dot{\boldsymbol{F}}\right)dH = \boldsymbol{\sigma}_{\alpha}^{r} \cdot \dot{\boldsymbol{\varepsilon}}_{\alpha}^{r}, \tag{51}$$

and the internal power can be evaluated through

$$P_{int} = \int_{V^{r}}\left(\boldsymbol{P} : \dot{\boldsymbol{F}}\right)dV^{r} = \int_{\Omega}\left(\boldsymbol{\sigma}_{\alpha}^{r} \cdot \dot{\boldsymbol{\varepsilon}}_{\alpha}^{r}\right)d\Omega\,. \tag{52}$$

The external power can be computed in the reference configuration by

$$\begin{aligned} P_{ext} = &\int_{\Omega^{r}}\left[\overline{\boldsymbol{t}}^{t} \cdot \dot{\boldsymbol{x}}^{t} + \overline{\boldsymbol{t}}^{b} \cdot \dot{\boldsymbol{x}}^{b} + \int_{H^{r}} \overline{\boldsymbol{b}} \cdot \dot{\boldsymbol{x}}dH\right]d\Omega^{r} \\ &+\int_{\Gamma_{t}^{r}}\int_{H^{r}} \overline{\boldsymbol{t}}^{l} \cdot \dot{\boldsymbol{x}}dH^{r}d\Gamma_{t}^{r} + \int_{\Gamma_{u}^{r}}\int_{H^{r}} \boldsymbol{r}^{r} \cdot \dot{\boldsymbol{x}}dH^{r}d\Gamma_{u}^{r}, \end{aligned} \tag{53}$$

where $\overline{\boldsymbol{t}}^{t}, \overline{\boldsymbol{t}}^{b}, \overline{\boldsymbol{t}}^{l}, \overline{\boldsymbol{b}}, \boldsymbol{r}^{r}$ are respectively the external surface tractions on the top, the bottom and the lateral surfaces of the shell, per unit reference area, the body force vector per unit reference volume and the generalized reaction on the kinematic boundary. The time differentiation of (27) yields $\dot{\boldsymbol{x}} = \dot{\boldsymbol{u}} + \left(\boldsymbol{\Gamma}\dot{\boldsymbol{\theta}}\right) \times \boldsymbol{a}$, so

$$\begin{aligned} P_{\text{ext}} = &\int_{\Omega^{r}}\left(\overline{\boldsymbol{q}}^{\Omega^{r}} \cdot \dot{\boldsymbol{d}}\right)d\Omega \\ &+\int_{\Gamma_{t}^{r}}\left(\overline{\boldsymbol{q}}^{\Gamma_{t}^{r}} \cdot \dot{\boldsymbol{d}}\right)d\Gamma_{t}^{r} + \int_{\Gamma_{u}^{r}}\left(\boldsymbol{q}^{\Gamma_{u}^{r}} \cdot \dot{\boldsymbol{d}}\right)d\Gamma_{u}^{r}, \end{aligned} \tag{54}$$

where

$$\overline{\boldsymbol{q}}^{\Omega^{r}} = \begin{bmatrix} \overline{\boldsymbol{n}}^{\Omega^{r}} \\ \boldsymbol{\Gamma}^{T}\overline{\boldsymbol{m}}^{\Omega^{r}} \end{bmatrix} \qquad \overline{\boldsymbol{q}}^{\Gamma_{t}^{r}} = \begin{bmatrix} \overline{\boldsymbol{n}}^{\Gamma_{t}^{r}} \\ \boldsymbol{\Gamma}^{T}\overline{\boldsymbol{m}}^{\Gamma_{t}^{r}} \end{bmatrix} \qquad \boldsymbol{q}^{\Gamma_{u}^{r}} = \begin{bmatrix} \boldsymbol{n}^{\Gamma_{u}^{r}} \\ \boldsymbol{\Gamma}^{T}\boldsymbol{m}^{\Gamma_{u}^{r}} \end{bmatrix}, \tag{55}$$

and $\boldsymbol{n}$ and $\boldsymbol{m}$ are resultants of force and moment respectively:

$$\begin{aligned} \overline{\boldsymbol{n}}^{\Omega^{r}} &= \overline{\boldsymbol{t}}^{tr} + \overline{\boldsymbol{t}}^{br} + \int_{H^{r}} \overline{\boldsymbol{b}}^{r}dH^{r} \\ \overline{\boldsymbol{m}}^{\Omega^{r}} &= \boldsymbol{a}^{t} \times \overline{\boldsymbol{t}}^{tr} + \boldsymbol{a}^{b} \times \overline{\boldsymbol{t}}^{br} + \int_{H^{r}} \boldsymbol{a} \times \overline{\boldsymbol{b}}^{r}dH^{r}, \end{aligned} \tag{56}$$

in the domain,

$$\begin{aligned} \overline{\boldsymbol{n}}^{\Gamma_t^r} &= \int_{H^r} \overline{\boldsymbol{t}}^{lr} dH^r \\ \overline{\boldsymbol{m}}^{\Gamma_t^r} &= \int_{H^r} \boldsymbol{a} \times \overline{\boldsymbol{t}}^{lr} dH^r \end{aligned}, \tag{57}$$

in the static boundary, and

$$\begin{aligned} \boldsymbol{n}^{\Gamma_u^r} &= \int_{H^r} \boldsymbol{r} dH^r \\ \boldsymbol{m}^{\Gamma_u^r} &= \int_{H^r} \boldsymbol{a} \times \boldsymbol{r} dH^r \end{aligned}, \tag{58}$$

for the reactions in the kinematic boundary.

3.4 Weak Form

Similarly to (52), one can define the internal virtual work as

$$\delta W_{int} = \int_{\Omega^r} \left(\boldsymbol{\sigma}_\alpha^r \cdot \delta \boldsymbol{\varepsilon}_\alpha^r \right) d\Omega \,, \tag{59}$$

where $\delta \boldsymbol{\varepsilon}_\alpha^r = \boldsymbol{\Psi}_\alpha \delta \boldsymbol{d}$ is a variation of the generalized strains. Also,

$$\delta W_{ext} = \int_{\Omega^r} \left(\overline{\boldsymbol{q}}^{\Omega^r} \cdot \delta \boldsymbol{d} \right) d\Omega + \int_{\Gamma_t^r} \left(\overline{\boldsymbol{q}}^{\Gamma_t^r} \cdot \delta \boldsymbol{d} \right) d\Gamma_t^r + \int_{\Gamma_u^r} \left(\boldsymbol{q}^{\Gamma_u^r} \cdot \delta \boldsymbol{d} \right) d\Gamma_u^r \,. \tag{60}$$

The compatibility in the essential boundary must be enforced in a weak statement, in this case, the complementary virtual work of the boundary reactions

$$-\int_{\Gamma_u^r} \delta \boldsymbol{q}^{\Gamma_u^r} \cdot \left(\boldsymbol{d} - \overline{\boldsymbol{d}} \right) d\Gamma_u^r = 0, \quad \forall \delta \boldsymbol{q}^{\Gamma_u^r} \,. \tag{61}$$

The final weak form is a combination of the principle of virtual work and this weak imposition, rendering the variation of a displacement functional

$$\begin{aligned} \delta W = &\int_{\Omega^r} \left(\boldsymbol{\sigma}_\alpha^r \cdot \delta \boldsymbol{\varepsilon}_\alpha^r \right) d\Omega^r - \int_{\Omega^r} \left(\overline{\boldsymbol{q}}^{\Omega^r} \cdot \delta \boldsymbol{d} \right) d\Omega - \int_{\Gamma_t^r} \left(\overline{\boldsymbol{q}}^{\Gamma_t^r} \cdot \delta \boldsymbol{d} \right) d\Gamma_t^r \\ &- \int_{\Gamma_u^r} \left(\boldsymbol{q}^{\Gamma_u^r} \cdot \delta \boldsymbol{d} \right) d\Gamma_u^r - \int_{\Gamma_u^r} \delta \boldsymbol{q}^{\Gamma_u^r} \cdot \left(\boldsymbol{d} - \overline{\boldsymbol{d}} \right) d\Gamma_u^r = 0 \quad \forall \delta \boldsymbol{d}, \delta \boldsymbol{q}^{\Gamma_u^r} \end{aligned} \,. \tag{62}$$

4 LINEAR SHELLS

4.1 Kinematics

The shells described in the previous chapter encompass finite displacement and rotations. This chapter assumes that, in the effective deformation, such quantities are small. This assumption can lead to a consistent linear formulation.

The displacement of any point in the shell can now be described as

$$\boldsymbol{\delta} = \boldsymbol{u} + \boldsymbol{\theta} \times \boldsymbol{a}^o \,. \tag{63}$$

This statement is equivalent to the linearization of (25) to the first order:

$$\boldsymbol{Q}^e = \boldsymbol{I} + \text{Skew}\left(\boldsymbol{\theta} \right). \tag{64}$$

The effective back-rotated strains can then be developed as in

$$
\begin{aligned}
\varepsilon_\alpha^r &= \begin{bmatrix} \boldsymbol{\eta}_\alpha^r \\ \boldsymbol{k}_\alpha^r \end{bmatrix} = \begin{bmatrix} \boldsymbol{Q}^T \boldsymbol{z}_{,\alpha} - \boldsymbol{e}_\alpha^r \\ \boldsymbol{k}_\alpha^{0r} + \boldsymbol{k}_\alpha^{er} \end{bmatrix} = \begin{bmatrix} \boldsymbol{Q}^{oT}\boldsymbol{Q}^{eT}\left(\boldsymbol{z}_{,\alpha}^o + \boldsymbol{u}_{,\alpha}\right) - \boldsymbol{e}_\alpha^r \\ \boldsymbol{k}_\alpha^{or} + \boldsymbol{Q}^T \boldsymbol{k}_\alpha^e \end{bmatrix} \\
&= \begin{bmatrix} \boldsymbol{Q}^{oT}\left(\boldsymbol{I} - \boldsymbol{\Theta}\right)\left(\boldsymbol{z}_{,\alpha}^o + \boldsymbol{u}_{,\alpha}\right) - \boldsymbol{e}_\alpha^r \\ \boldsymbol{k}_\alpha^{or} + \boldsymbol{Q}^{oT}\boldsymbol{Q}^{eT}\boldsymbol{\Gamma}\boldsymbol{\theta}_{,\alpha} \end{bmatrix} \\
&= \begin{bmatrix} \boldsymbol{Q}^{oT}\left(\boldsymbol{z}_{,\alpha}^o + \boldsymbol{u}_{,\alpha} - \boldsymbol{\Theta}\boldsymbol{z}_{,\alpha}^o - \boldsymbol{\Theta}\boldsymbol{u}_{,\alpha}\right) - \boldsymbol{e}_\alpha^r \\ \boldsymbol{k}_\alpha^{or} + \boldsymbol{Q}^{oT}\left(\boldsymbol{I} - \boldsymbol{\Theta}\right)\boldsymbol{\Gamma}\boldsymbol{\theta}_{,\alpha} \end{bmatrix} \qquad \left(\text{neglecting } \boldsymbol{\Theta}\boldsymbol{u}_{,\alpha}\right) \\
&= \begin{bmatrix} \boldsymbol{Q}^{oT}\boldsymbol{z}_{,\alpha}^o + \boldsymbol{Q}^{oT}\left(\boldsymbol{u}_{,\alpha} + \boldsymbol{z}_{,\alpha}^o \times \boldsymbol{\theta}\right) - \boldsymbol{e}_\alpha^r \\ \boldsymbol{k}_\alpha^{or} + \boldsymbol{Q}^{oT}\left(\boldsymbol{\Gamma}\boldsymbol{\theta}_{,\alpha} - \boldsymbol{\Theta}\boldsymbol{\Gamma}\boldsymbol{\theta}_{,\alpha}\right) \end{bmatrix} \qquad \begin{pmatrix} \text{neglecting } \boldsymbol{\Theta}\boldsymbol{\Gamma}\boldsymbol{\theta}_{,\alpha} \\ \text{taking } \boldsymbol{\Gamma} \cong \boldsymbol{I} \end{pmatrix}, \\
&= \begin{bmatrix} \boldsymbol{\eta}_\alpha^{or} + \boldsymbol{Q}^{oT}\left(\boldsymbol{u}_{,\alpha} + \boldsymbol{z}_{,\alpha}^o \times \boldsymbol{\theta}\right) \\ \boldsymbol{k}_\alpha^{or} + \boldsymbol{Q}^{oT}\boldsymbol{\theta}_{,\alpha} \end{bmatrix} \\
&= \varepsilon_\alpha^{or} + \begin{bmatrix} \boldsymbol{Q}^{oT} & \boldsymbol{0} \\ \boldsymbol{0} & \boldsymbol{Q}^{oT} \end{bmatrix} \begin{bmatrix} \boldsymbol{I} & \boldsymbol{0} & \boldsymbol{Z}_{,\alpha}^o \\ \boldsymbol{0} & \boldsymbol{I} & \boldsymbol{0} \end{bmatrix} \begin{bmatrix} \boldsymbol{u}_{,\alpha} \\ \boldsymbol{\theta}_{,\alpha} \\ \boldsymbol{\theta} \end{bmatrix}
\end{aligned} \tag{65}
$$

where $\varepsilon_\alpha^{or} = \begin{bmatrix} \boldsymbol{\eta}_\alpha^{or} & \boldsymbol{\kappa}_\alpha^{or} \end{bmatrix}^T$ collects the initial strains and $\boldsymbol{Z}_{,\alpha}^o = \mathrm{Skew}\left(\boldsymbol{z}_{,\alpha}^o\right)$. The same results arise from expanding ε_α^r and neglecting higher order terms:

$$
\begin{aligned}
\varepsilon_\alpha^r &\cong \varepsilon_\alpha^r\Big|_{\boldsymbol{d}=\boldsymbol{0}} + \left.\frac{\partial \varepsilon_\alpha^r}{\partial \boldsymbol{d}}\right|_{\boldsymbol{d}=\boldsymbol{0}} \boldsymbol{d} \\
&= \varepsilon_\alpha^{or} + \boldsymbol{\Psi}_\alpha\Big|_{\boldsymbol{d}=\boldsymbol{0}} \boldsymbol{\Delta}_\alpha \boldsymbol{d} \\
&= \varepsilon_\alpha^{or} + \boldsymbol{\Psi}_\alpha^o \boldsymbol{\Delta}_\alpha \boldsymbol{d}
\end{aligned} \quad . \tag{66}
$$

Any variation may only be done in the effective part of ε_α^r, e.g.

$$
\delta\varepsilon_\alpha^r = \boldsymbol{\Psi}_\alpha^o \boldsymbol{\Delta}_\alpha \delta\boldsymbol{d} \quad . \tag{67}
$$

The back-rotated effective strain can now be expressed, after some algebra, by

$$
\boldsymbol{\gamma}_\alpha^{\mathrm{e}r} = J^{o-1}\left(\boldsymbol{e}_\alpha^r \cdot \boldsymbol{g}_\beta^{\mathrm{o}r}\right)\left(\boldsymbol{\eta}_\beta^{er} + \boldsymbol{\kappa}_\beta^{er} \times \boldsymbol{a}^r\right) \tag{68}
$$

where the effective back-rotated cross-sectional strains

$$
\begin{aligned}
\boldsymbol{\eta}_\alpha^{er} &= \boldsymbol{Q}^{oT}\boldsymbol{\eta}_\alpha^e = \boldsymbol{Q}^{oT}\left(\boldsymbol{u}_{,\alpha} + \boldsymbol{z}_{,\alpha}^o \times \boldsymbol{\theta}\right) \\
\boldsymbol{\kappa}_\alpha^{er} &= \boldsymbol{Q}^{oT}\boldsymbol{\kappa}_\alpha^e = \boldsymbol{Q}^{oT}\boldsymbol{\theta}_{,\alpha}
\end{aligned} \quad , \tag{69}
$$

were defined.

4.2 Linear Material

After the imposition of plane stress, and proper linearization, the material constants are a generalized Hooke law, e.g.

$$
\boldsymbol{\tau}_\alpha^{\mathrm{e}r} = \left[\frac{E}{2\left(1-\nu\right)} \boldsymbol{e}_\alpha^r \otimes \boldsymbol{e}_\beta^r\right] \boldsymbol{\gamma}_\beta^{\mathrm{e}r} + \frac{E}{2\left(1+\nu\right)} \varepsilon_{\alpha\beta} \boldsymbol{E}_3^r \boldsymbol{\gamma}_\beta^{\mathrm{e}r} + \frac{E}{2\left(1+\nu\right)} \boldsymbol{\gamma}_\alpha^{\mathrm{e}r} \quad . \tag{70}
$$

or $\boldsymbol{\tau}_\alpha^{\mathrm{e}r} = \boldsymbol{C}_{\alpha\beta}^{er} \boldsymbol{\gamma}_\beta^{\mathrm{e}r}$. Using E the Young modulus and ν the Poisson's ratio.

$$\boldsymbol{C}_{11}^{er} = \frac{E}{2\left(1+\nu\right)}\begin{bmatrix} \dfrac{2}{\left(1-\nu\right)} & \cdot & \cdot \\ \cdot & 1 & \cdot \\ \cdot & \cdot & 1 \end{bmatrix}, \quad \boldsymbol{C}_{12}^{er} = \frac{E}{2\left(1+\nu\right)}\begin{bmatrix} \cdot & \dfrac{2\nu}{\left(1-\nu\right)} & \cdot \\ 1 & \cdot & \cdot \\ \cdot & \cdot & \cdot \end{bmatrix}, \tag{71}$$

$$\boldsymbol{C}_{21}^{er} = \boldsymbol{C}_{12}^{erT}, \qquad \boldsymbol{C}_{22}^{er} = \frac{E}{2\left(1+\nu\right)}\begin{bmatrix} 1 & \cdot & \cdot \\ \cdot & \dfrac{2}{\left(1-\nu\right)} & \cdot \\ \cdot & \cdot & 1 \end{bmatrix}.$$

The linear relation between the generalized strains and generalized effective stresses (all of those in their back-rotated forms) can be expressed by

$$\begin{aligned} \boldsymbol{\sigma}_{\alpha}^{r} &= \boldsymbol{D}_{\alpha\beta}\boldsymbol{\varepsilon}_{\beta}^{er} \\ \boldsymbol{D}_{\alpha\beta} &= \frac{\partial \boldsymbol{\sigma}_{\alpha}^{r}}{\partial \boldsymbol{\varepsilon}_{\beta}^{er}} = \begin{bmatrix} \dfrac{\partial \boldsymbol{n}_{\alpha}^{r}}{\partial \boldsymbol{\eta}_{\beta}^{er}} & \dfrac{\partial \boldsymbol{n}_{\alpha}^{r}}{\partial \boldsymbol{\kappa}_{\beta}^{er}} \\ \dfrac{\partial \boldsymbol{m}_{\alpha}^{r}}{\partial \boldsymbol{\eta}_{\beta}^{er}} & \dfrac{\partial \boldsymbol{m}_{\alpha}^{r}}{\partial \boldsymbol{\kappa}_{\beta}^{er}} \end{bmatrix}, \end{aligned} \tag{72}$$

whose components can be obtained through the use of (46), (68), (70) and the chain rule and are summarized in

$$\frac{\partial \boldsymbol{n}_{\alpha}^{r}}{\partial \boldsymbol{\eta}_{\beta}^{er}} = \int_{H}\left(J^{o-1}\left(\boldsymbol{g}_{\alpha}^{or}\cdot\boldsymbol{e}_{\delta}^{r}\right)\boldsymbol{C}_{\delta\gamma}^{er}\left(\boldsymbol{e}_{\gamma}^{r}\cdot\boldsymbol{g}_{\beta}^{or}\right)\right)d\xi_3\,. \tag{73}$$

$$\frac{\partial \boldsymbol{n}_{\alpha}^{r}}{\partial \boldsymbol{\kappa}_{\beta}^{er}} = -\int_{H}\left(J^{o-1}\left(\boldsymbol{g}_{\alpha}^{or}\cdot\boldsymbol{e}_{\delta}^{r}\right)\boldsymbol{C}_{\delta\gamma}^{er}\left(\boldsymbol{e}_{\gamma}^{r}\cdot\boldsymbol{g}_{\beta}^{or}\right)\boldsymbol{A}^{r}\right)d\xi_3\,. \tag{74}$$

$$\frac{\partial \boldsymbol{m}_{\alpha}^{r}}{\partial \boldsymbol{\eta}_{\beta}^{er}} = \int_{H}\left(J^{o-1}\boldsymbol{A}^{r}\left(\boldsymbol{g}_{\alpha}^{or}\cdot\boldsymbol{e}_{\delta}^{r}\right)\boldsymbol{C}_{\delta\gamma}^{er}\left(\boldsymbol{e}_{\gamma}^{r}\cdot\boldsymbol{g}_{\beta}^{or}\right)\right)d\xi_3 = \left(\frac{\partial \boldsymbol{n}_{\alpha}^{r}}{\partial \boldsymbol{\kappa}_{\beta}^{er}}\right)^{T}. \tag{75}$$

$$\frac{\partial \boldsymbol{m}_{\alpha}^{r}}{\partial \boldsymbol{\kappa}_{\beta}^{er}} = -\int_{H}\left(J^{o-1}\boldsymbol{A}^{r}\left(\boldsymbol{g}_{\alpha}^{or}\cdot\boldsymbol{e}_{\delta}^{r}\right)\boldsymbol{C}_{\delta\gamma}^{er}\left(\boldsymbol{e}_{\gamma}^{r}\cdot\boldsymbol{g}_{\beta}^{or}\right)\boldsymbol{A}^{r}\right)d\xi_3\,. \tag{76}$$

4.3 Shallow Shells

A problem arises with the integrations in (73)-(76) through the thickness. The quantities J^o and $\boldsymbol{g}_{\alpha}^{or}$ vary along ξ_3 and a numerical quadrature along this axis should be avoided.

Symbolic development for some types of initial mapping proved that, given that $r >> h$,e.g., the curvature radius of the initial mapping is much bigger than the thickness of the shell, those quantities can be taken as constant and evaluated only in the midsurface.

This procedure is equivalent to a one point quadrature rule and results yet to be published prove that this assumption is valid even for r not much bigger than h.

The resulting expressions for the components of $\boldsymbol{D}$ are

$$\begin{aligned}
\frac{\partial \boldsymbol{n}_\alpha^r}{\partial \boldsymbol{\eta}_\beta^{er}} &= hJ^{o-1}\left(\boldsymbol{g}_\alpha^{or}\cdot\boldsymbol{e}_\delta^r\right)\left(\boldsymbol{e}_\gamma^r\cdot\boldsymbol{g}_\beta^{or}\right)\boldsymbol{C}_{\delta\gamma}^{er} \\
\frac{\partial \boldsymbol{n}_\alpha^r}{\partial \boldsymbol{\kappa}_\beta^{er}} &= \left(\frac{\partial \boldsymbol{m}_\alpha^r}{\partial \boldsymbol{\eta}_\beta^{er}}\right)^T = \boldsymbol{0} \\
\frac{\partial \boldsymbol{m}_\alpha^r}{\partial \boldsymbol{\kappa}_\beta^{er}} &= -\frac{h^3}{12}J^{o-1}\left(\boldsymbol{g}_\alpha^{or}\cdot\boldsymbol{e}_\delta^r\right)\left(\boldsymbol{e}_\gamma^r\cdot\boldsymbol{g}_\beta^{or}\right)\boldsymbol{E}_3^r\boldsymbol{C}_{\delta\gamma}^{er}\boldsymbol{E}_3^r
\end{aligned} \quad , \tag{1.77}$$

with J^o and $\boldsymbol{g}_\alpha^{or}$ evaluated at the midsurface.

These results can also be applied to approximated initial mappings, in which $\boldsymbol{z}^o$ can be approximated, for instance, from a set of points collected from an actual shell model.

5 APPROXIMATION WITH ELEMENT-FREE GALERKIN (EFG)

Both the geometrically exact and the linear theory are developed without great consideration of the approximation method to be used. Apart from the inclusion of the reactions in the essential boundary in the external virtual work and from the weak imposition of the compatibility therein (both needed for non-interpolatory approximations such as Moving Least Squares), no further observation is made concerning the trial and test spaces.

For this work, a Meshless Method is chosen: the Element-Free Galerkin, as described in Belytschko *et al*. (1994), which consists of approximating the trial and test spaces with Moving Least Squares (computer implementation is actually done with MFLS, as described in section 2.2).

So, gathering the shape functions as follows

$$\boldsymbol{\Phi}^{\Omega}\left(\boldsymbol{x}\right) = \left[\mathbf{I}_6\Phi_1\left(\boldsymbol{x}\right) \quad \mathbf{I}_6\Phi_2\left(\boldsymbol{x}\right) \quad \cdots \quad \mathbf{I}_6\Phi_n\left(\boldsymbol{x}\right)\right], \tag{78}$$

where $\mathbf{I}_6$ is the identity matrix of order 6 and $\Phi_i\left(\boldsymbol{x}\right)$ is the shape function associated to the particle i evaluated at point $\boldsymbol{x}$, and defining

$$\mathbf{u} = \left\{\mathrm{u}_{01} \quad \mathrm{u}_{02} \quad \mathrm{u}_{03} \quad \mathrm{u}_{04} \quad \mathrm{u}_{05} \quad \mathrm{u}_{06} \quad \mathrm{u}_{07} \quad \mathrm{u}_{08} \quad \mathrm{u}_{09} \quad \mathrm{u}_{10} \quad \mathrm{u}_{11} \quad \mathrm{u}_{12} \quad \cdots\right\}^T \tag{79}$$

the set of nodal parameters, the domain approximation for the displacements, the rotations and the virtual counterparts are

$$\boldsymbol{d}\left(\boldsymbol{x}\right) = \begin{Bmatrix} u_1\left(\boldsymbol{x}\right) \\ u_2\left(\boldsymbol{x}\right) \\ u_3\left(\boldsymbol{x}\right) \\ \theta_1\left(\boldsymbol{x}\right) \\ \theta_2\left(\boldsymbol{x}\right) \\ \theta_3\left(\boldsymbol{x}\right) \end{Bmatrix} = \boldsymbol{\Phi}^{\Omega}\left(\boldsymbol{x}\right)\mathbf{u} \quad . \tag{80}$$

$$\delta\boldsymbol{d}\left(\boldsymbol{x}\right) = \boldsymbol{\Phi}^{\Omega}\left(\boldsymbol{x}\right)\delta\mathbf{u}$$

In the kinematic boundary, the reaction resultants can are interpolated with linear Lagrange polynomials. The trial and test spaces for the reactions are then

$$\boldsymbol{q}^{\Gamma_u}\left(\boldsymbol{x}_u\right)=\begin{Bmatrix} n_1^{\Gamma_u^r}\left(\boldsymbol{x}_u\right)\\ n_2^{\Gamma_u^r}\left(\boldsymbol{x}_u\right)\\ n_3^{\Gamma_u^r}\left(\boldsymbol{x}_u\right)\\ \mu_1^{\Gamma_u^r}\left(\boldsymbol{x}_u\right)\\ \mu_2^{\Gamma_u^r}\left(\boldsymbol{x}_u\right)\\ \mu_3^{\Gamma_u^r}\left(\boldsymbol{x}_u\right)\end{Bmatrix}=\boldsymbol{\Phi}^{\Gamma}\left(\boldsymbol{x}_u\right)\mathbf{r}\,, \tag{81}$$

$$\delta\boldsymbol{q}^{\Gamma_u}\left(\boldsymbol{x}_u\right)=\boldsymbol{\Phi}^{\Gamma}\left(\boldsymbol{x}_u\right)\delta\mathbf{r}$$

where $\boldsymbol{x}_u$ is a point in the essential border.

The resulting discretized version of the weak form (62) is

$$\begin{aligned}\delta W=\;&\boldsymbol{\delta}\mathbf{u}^T\int_{\Omega^r}\left(\left(\boldsymbol{\Psi}^o_{\alpha}\boldsymbol{\Lambda}_{\alpha}\boldsymbol{\Phi}^{\Omega}\right)^T\mathbf{D}_{\alpha\beta}\boldsymbol{\Psi}^o_{\beta}\boldsymbol{\Lambda}_{\beta}\boldsymbol{\Phi}^{\Omega}\right)d\Omega^r\mathbf{u}\\ &-\boldsymbol{\delta}\mathbf{u}^T\int_{\Omega^r}\left(\boldsymbol{\Phi}^{\Omega T}\overline{\mathbf{q}}^{\Omega^r}\right)d\Omega-\boldsymbol{\delta}\mathbf{u}^T\int_{\Gamma_t^r}\left(\boldsymbol{\Phi}^{\Omega T}\overline{\mathbf{q}}^{\Gamma_t^r}\right)d\Gamma_t^r\\ &-\boldsymbol{\delta}\mathbf{u}^T\int_{\Gamma_u^r}\left(\boldsymbol{\Phi}^{\Omega T}\boldsymbol{\Phi}^{\Gamma}\right)d\Gamma_u^r\mathbf{r}\\ &-\boldsymbol{\delta}\mathbf{r}^T\int_{\Gamma_u^r}\boldsymbol{\Phi}^{\Gamma T}\boldsymbol{\Phi}^{\Omega}d\Gamma_u^r\mathbf{u}+\boldsymbol{\delta}\mathbf{r}^T\int_{\Gamma_u^r}\boldsymbol{\Phi}^{\Gamma T}\overline{\mathbf{d}}\,d\Gamma_u^r=0\qquad,\forall\boldsymbol{\delta}\mathbf{u},\boldsymbol{\delta}\mathbf{r}\end{aligned}\;. \tag{82}$$

As (82) is valid for every variation $\boldsymbol{\delta}\mathbf{u},\boldsymbol{\delta}\mathbf{r}$, it renders the linear system of equations

$$\begin{bmatrix}\mathbf{K} & \mathbf{G}\\ \mathbf{G}^T & \mathbf{0}\end{bmatrix}\begin{Bmatrix}\mathbf{u}\\ \mathbf{r}\end{Bmatrix}=\begin{Bmatrix}\mathbf{f}\\ \mathbf{q}\end{Bmatrix}$$

with

$$\begin{aligned}\mathbf{K}&=\int_{\Omega^r}\left(\left(\boldsymbol{\Psi}^o_{\alpha}\boldsymbol{\Lambda}_{\alpha}\boldsymbol{\Phi}^{\Omega}\right)^T\mathbf{D}_{\alpha\beta}\boldsymbol{\Psi}^o_{\beta}\boldsymbol{\Lambda}_{\beta}\boldsymbol{\Phi}^{\Omega}\right)d\Omega^r\\ \mathbf{G}&=\int_{\Gamma_u^r}\boldsymbol{\Phi}^{\Gamma T}\boldsymbol{\Phi}^{\Gamma}d\Gamma_u^r\\ \mathbf{f}&=\int_{\Omega^r}\mathbf{q}^{\Omega T}d\Omega+\int_{\Gamma_t^r}\boldsymbol{\Phi}^{\Gamma T}\overline{\mathbf{q}}^{\Gamma_t^r}d\Gamma_t^r\\ \mathbf{q}&=\int_{\Gamma_u^r}\boldsymbol{\Phi}^{\Gamma T}\overline{\mathbf{d}}^{\Gamma_u^r}d\Gamma_u^r\end{aligned}\;. \tag{83}$$

6 NUMERICAL EXAMPLES

6.1 Cantilever beam

$P = 1,$
$E = 10^6,$
$\nu = 0,3$

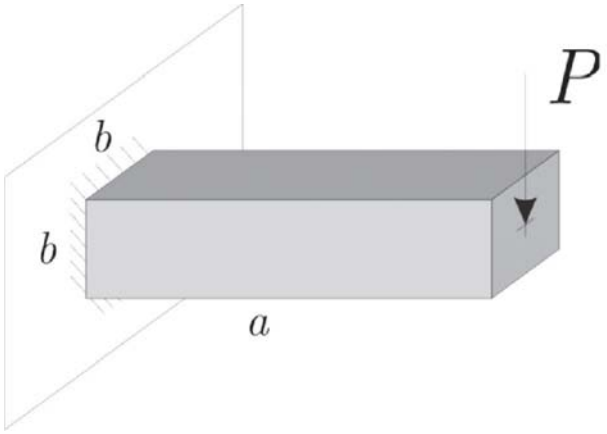

Figure 2: Cantilever beam with end load

The simulation of the cantilever depicted in Figure 2 can be done with two different models:
Type 1, depicted in Figure 3, is a plane stress flat shell with the load in its own plane, and Type 2, as shown in Figure 4 is a flat plate, also under plane stress assumption, with the load acting on a plane normal to the shell.

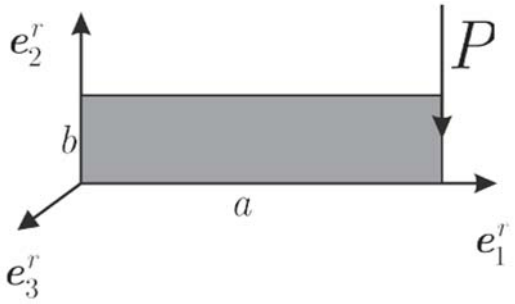

Figure 3: Cantilever - Model 1

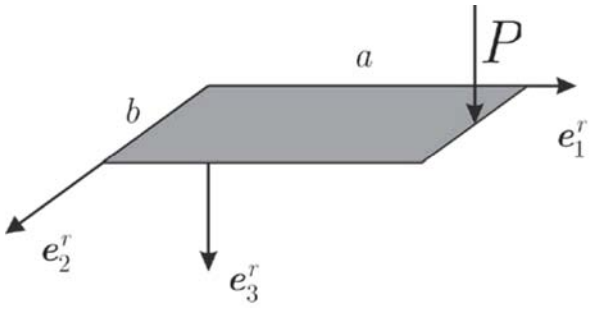

Figure 4: Cantilever - Model 2

The load and material properties are show in Figure 2. In order for the different models to be compared, the cross-section was taken square ($b = 2$). The results are compared against the solution for an equivalent Timoshenko rod model, so the length was taken sufficiently large in comparison to the cross-sectional dimensions ($a = 20$). The model differs from that in the Timoshenko rod theory, so results are only for a loose comparison and are given by

$$w = \frac{Pa^3}{3EI} + \frac{Pa}{GA'},$$
$$G = \frac{E}{2\left(1+\nu\right)}, I = \frac{bh^3}{12}, A' = \frac{5}{6}b^2 \tag{84}$$

The integration of the weak form is done in the reference configuration using the 250 cell structure depicted in Figure 5, each cell with 3 integration points in each direction e_α^T.

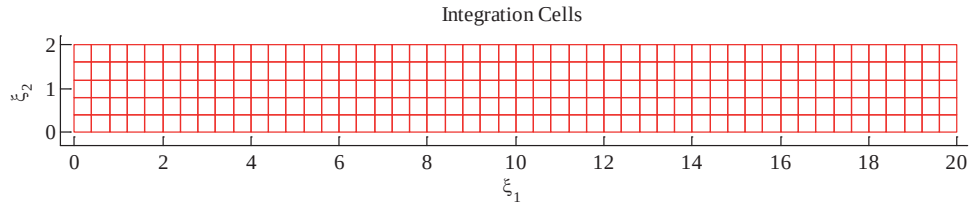

Figure 5: Cantilever - Integration cells

The Moving Least Squares approximation was done with a full bi-quadratic polynomial base and the particle support was amplified by 1.5. Simulations were carried out for 4 different particle distributions as seen in Figure 6.

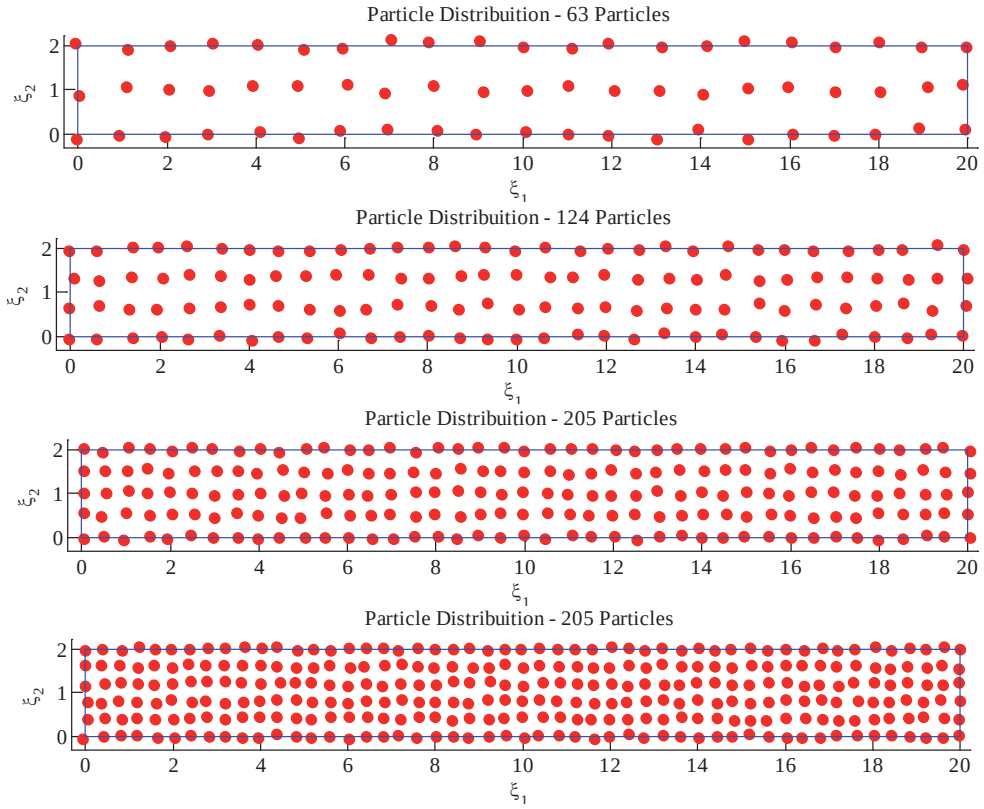

Figure 6: Cantilever - Particle distribution

A random noise was introduced in the particle distributions. It improves the solution as linear dependencies arising from co-linear particles are minimized. The results, normalized by the Timoshenko beam displacement at the load application point are given in Figure 7.

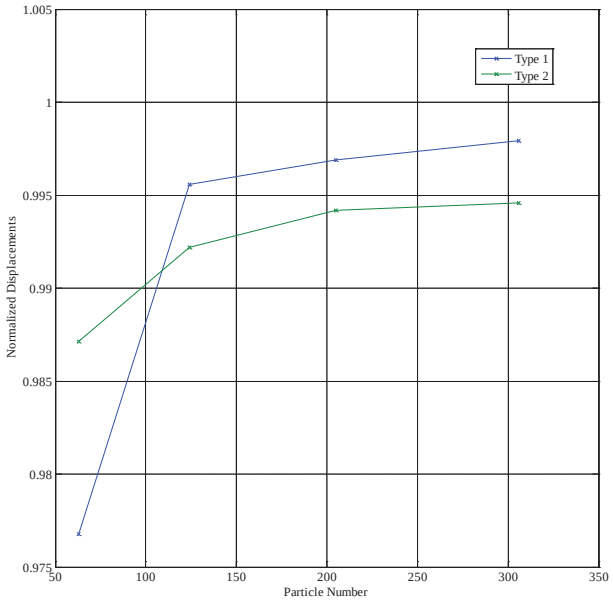

Figure 7: Cantilever - Results

6.2 Flate Plate

A flat plate with uniform load, as shown in Figure 8 was simulated.

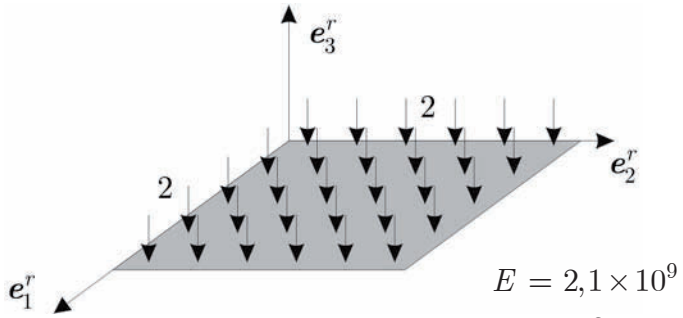

Figure 8: Flat Plate

The material's properties are indicated in the picture. The support was considered as to be of the simple hard kind, e.g., the displacements in the vertical direction were constrained, and so were the rotations normal to the borders. The load was taken to be 6.25×10^4 times the thickness.

The number of integration cells now varies with the particle distribution, as shown in Figure 9 for the 36 particles case. 7 different particle distributions were simulated, all with a complete 4^{th} order polynomial base and support amplification factor 1.75.

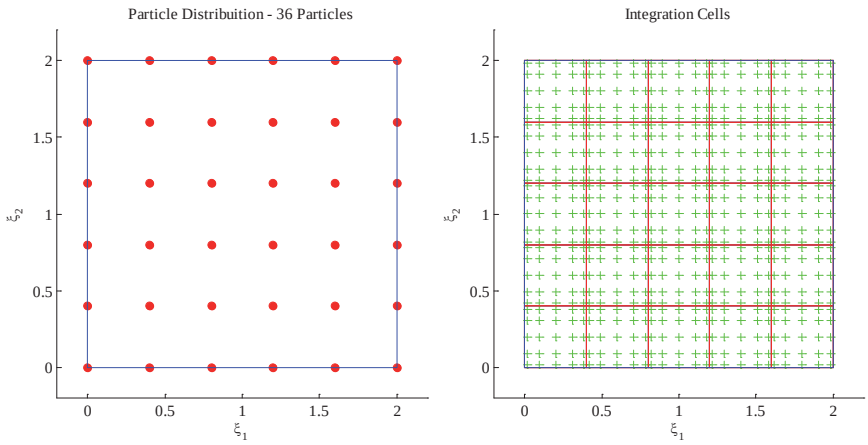

Figure 9: Flat Plate - Particle distribuiton and Integration cells

Results are depicted in Figure 10. It's interesting to note a loss of accuracy in the most slender plate. It's probably due to the fact that, in this meshless method, the approximation space obtained with a finer particle distribution doesn't always contain that generated by a coarser distribution, hence, the error can't be easily assessed.

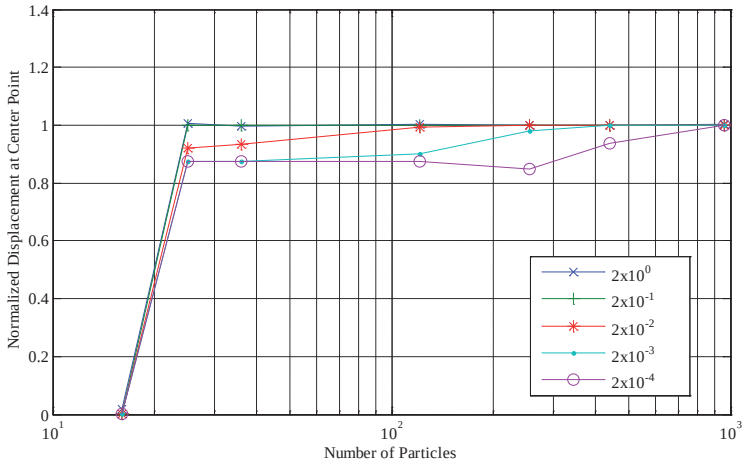

Figure 10: Flat Plate - Results

6.3 Cylindrical Shell with Border Moment

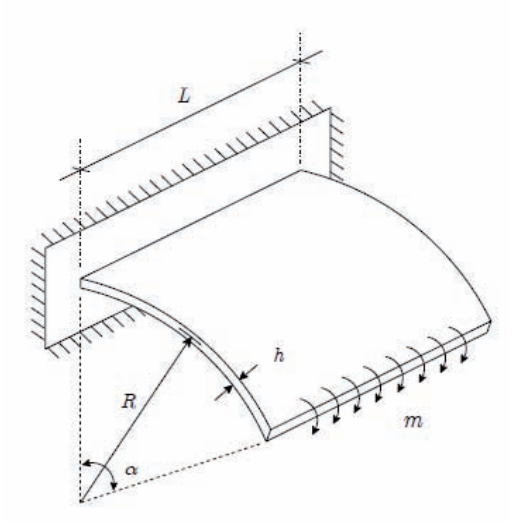

$$R = 2$$
$$\alpha = 30^{o}$$
$$L = 1,0$$
$$m = 240$$
$$E = 2,1 \times 10^{9}$$
$$\nu = 0,0$$

Figure 11: Cylindrical Shell

This example was taken from Campello (2005) where it was approximated with triangular finite elements.

8 different particle distributions and integration cells were used, in the same fashion as the previous examples. This time, 5 different thicknesses were simulated.

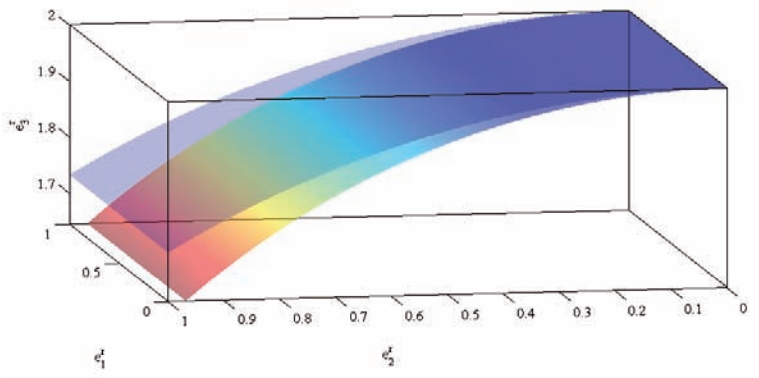

Figure 12: Cylindrical Shell - Deformed shape (displacements are amplified)

An example of a deformed shape is given by Figure 12 and the result for the various thicknesses studied is in Figure 13. The presence of membrane locking can be seen for the shell whose thickness is 10^{-4} times the initial curvature. This was easily removed by enlarging the polynomial base to a complete 3rd order bi-dimensional one.

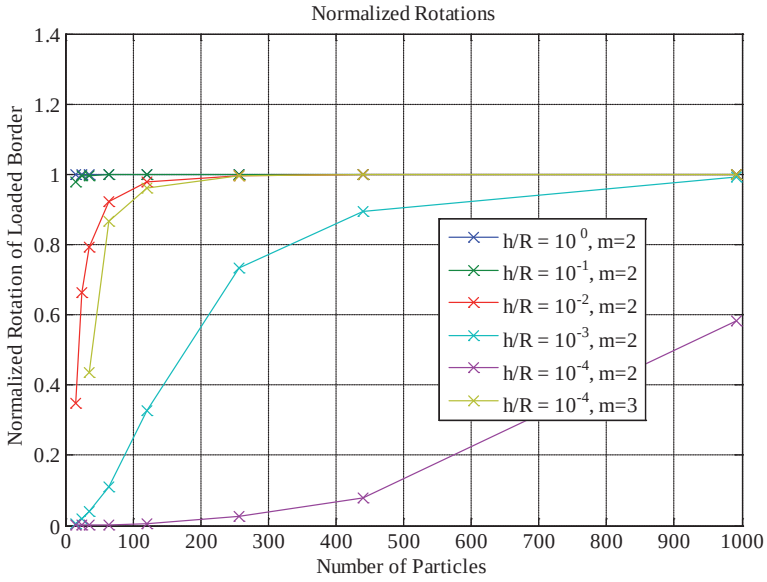

Figure 13: Cylindrical Shell - Results

6.4 Pinched Cylinder

The pinched cylinder analyzed in Simo *et al.* (1989) is here represented in Figure 14 with the geometrical and load parameters. The unitary load corresponds to the full model. The discretized model, considering the symmetry, uses a quarter of that.

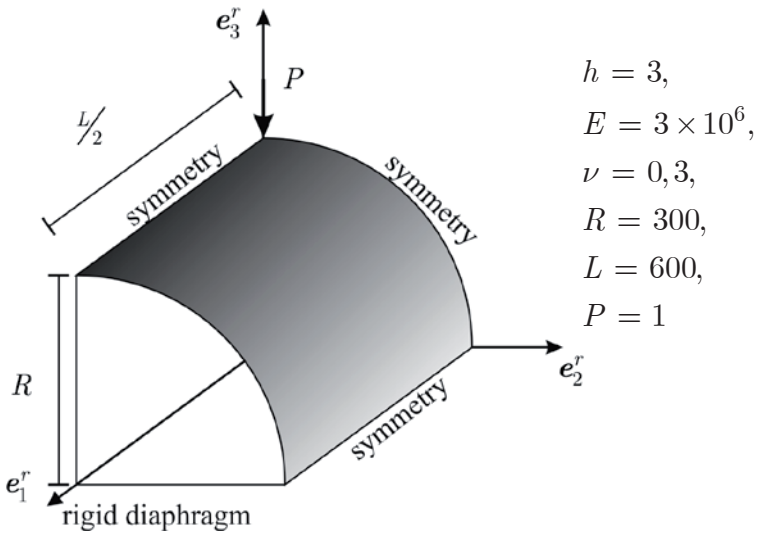

Figure 14: Pinched Cylinder

The simulations are carried out in the same fashion as the previous examples, but only for one thickness. A convergence study is shown in Figure 15 along with a deformed shape, with displacements amplified by 10^7.

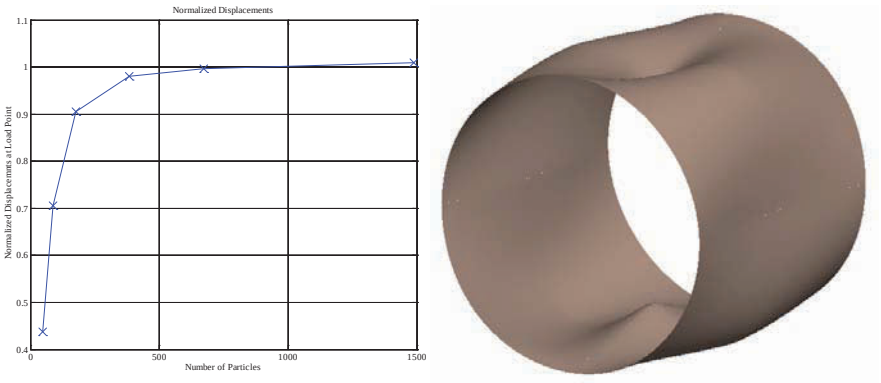

Figure 15: Pinched Cylinder- Convergence and deformed shape

6.5 Pinched Hemispherical Shell

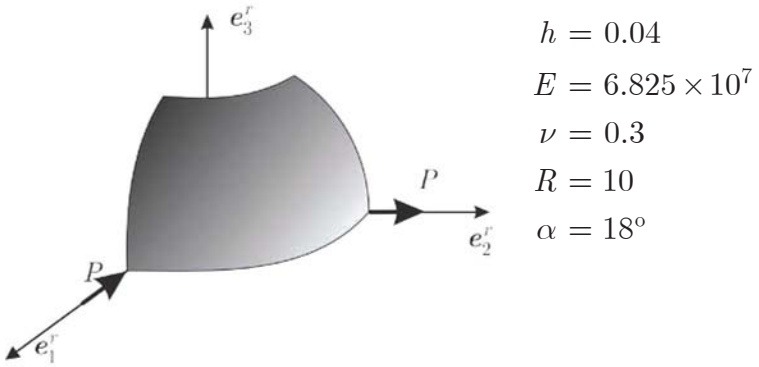

Figure 16: Pinched Hemispherical Shell

The pinched hemispherical shell with a 18° hole example in Figure 16 is also present in Simo *et al.* (1989). It was analyzed with 6 different particle and integration cell distribution, such as that in Figure 17. Two different views of the deformed shape can be seen in Figure 17.

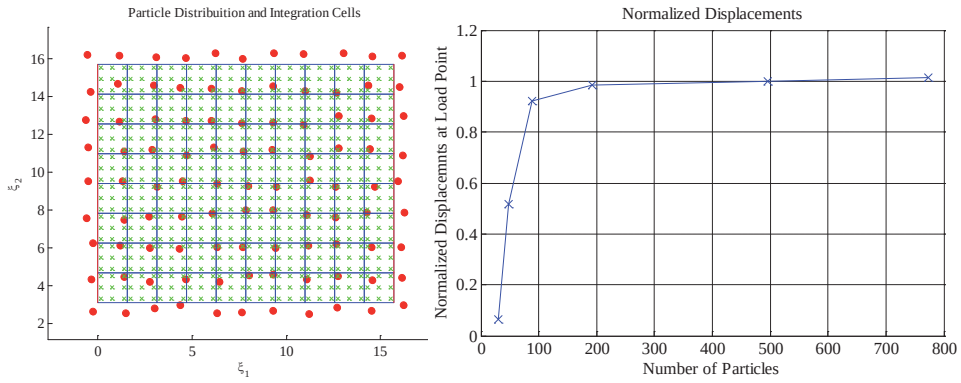

Figure 17: Pinched Hemispheric - Particle distribution and convergence

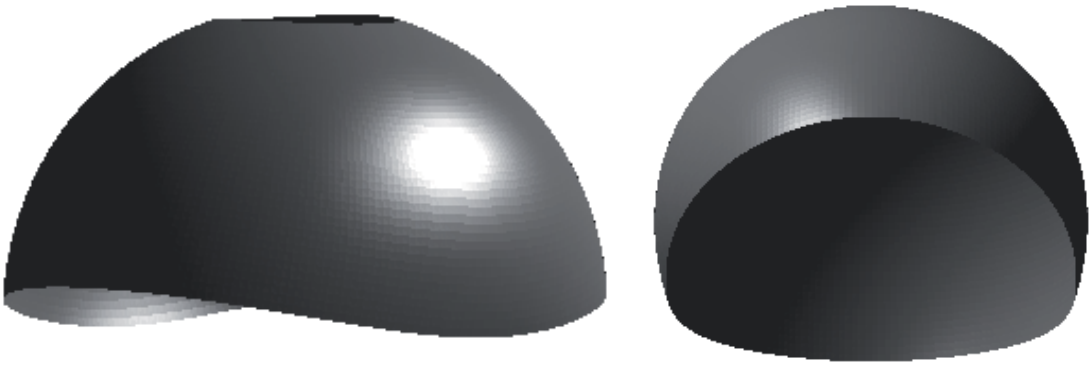

Figure 18: Pinched Hemispheric - Deformed shape

6.6 Full Hemispherical Shell

The results for the previous example, without the hole on the top can be seen in Figure 19 and the deformed shape in Figure 20.

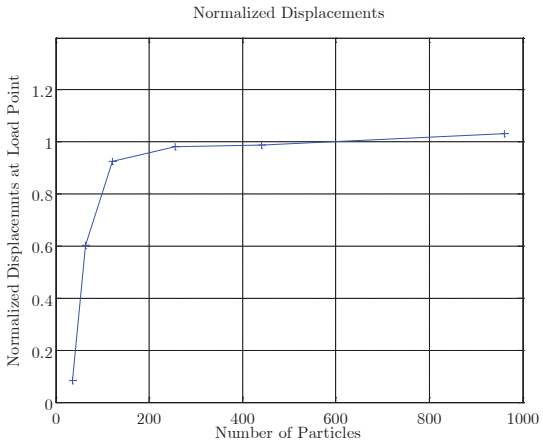

Figure 19: Full Hemispherical Shell – Results

Figure 20: Full Hemispherical Shell - Deformed shapes

7 CONCLUSIONS

The Element-Free Galerkin Method can provide smooth results for the structural analysis of shells. Actually, the desired smoothness for the displacements (and consequently for the strains and stresses) can be imposed using the appropriate weight function. Shell structures seem to be

one of the most prominent fields of application of such methods due to the nature of shell behavior. This type of approximation combined with the used shell theory allows for the exact description of the shell initial configuration.

The method also proved useful when a necessary improvement of the approximation base. The size of the polynomial base can be easily increased. In a FEM approach, a re-meshing procedure would have to be at hand for this kind of refinement.

Some losses can be accounted for as the shape functions aren't as simple as those used by FEM. The integration isn't exact and the computational cost is raised by a wider connectivity (the stiffness matrix is not as sparse as those in FEM). The numerical computation of the shape functions is also demanding.

The linear shell theory derived is consistent and presented in a neatly way. The resulting system of equations resembles that of a plate problem, with changes in the constitutive relation and a distribution matrix $\boldsymbol{\Psi}_{\alpha}^{o}$. It's also suitable for meshless implementation as it maintains the main characteristics of the original theory.

The numerical examples exhibit good convergence to the reference solutions, what validates the theory.

8 ACKNOLEDGEMENTS

The first author acknowledge his master studies funding by FAPESP (*Fundação de Amparo à Pesquisa do Estado de São Paulo*) under grant number 2009/04525-5. The third author acknowledges the *Mercator Gastprofessur* from the DFG (*Deutsche Forschungsgemeinschaft*) that made possible his stay at the IBNM (Institute of Mechanics and Computational Mechanics, Leibniz University of Hannover) on a leave from the University of São Paulo, as well as the support by CNPq (*Conselho Nacional de Desenvolvimento Tecnológico*) under the grant 305822/2006-3.

REFERENCES

Belytschko T, Lu YY and Gu L. *Element-Free Galerkin Methods.* International Journal for Numerical Methods in Engineering, 37. Wiley InterScience, 1994.

Campello EMB, Pimenta PM and Wriggers P. *A geometrically-exact finite strain shell model for the analysis of initially curved shells.* Sixth World Congress on Computational Mechanics Second Asian-Pacific Congress on Computational Mechanics. Tsinghua University Press & Springer-Verlag, Beijing, China, 2004.

Campello EMB. *Modelos não-lineares de casca em elasticidade e elastoplasticidade com grandes deformações: teoria e implementação em elementos finitos*. Ph.D. Thesis (in portuguese). Escola Politécnica da Universidade de São Paulo. São Paulo, 2005.

Li S and Liu WK. *Meshfree Particle Methods.* Springer. Berkeley and Evanston, EUA, 2004.

Pimenta PM and Campelo EMB. *Shell curvature as an initial deformation: A geometrically exact finite element approach.* International Journal for Numerical Methods in Engineering. Wiley InterScience, 2009.

Pimenta PM and Yojo T. *Geometrically-exact analysis of spatial frames.* Appl Mech Reviews, ASME, 46(11), pp. 118–128, 1993.

Pimenta PM. *Geometrically exact analysis of initially curved rods*. In: Advances in Computational Techniques for Structural Engineering. Topping H. V. (editor), vol. 1. Civil-Comp: Edinburgh, Reino Unido, 1996.

Pimenta PM. *On a geometrically-exact finite-strain shell model*. Proceedings of the 3rd Pan-American Congress on Applied Mechanics, III (PACAM), São Paulo, 1993.

Simo JC, Fox DD and Rifai M. *On a stress resultant geometrically exact shell model. Part II: the linear theory; computational aspects*. Computer Methods in Applied Mechanics and Engineering, 73(1), 1989.

Simo JC. *A finite strain beam formulation. Part I: The three-dimensional dynamic problem*. Comput. Meth Appl Mech Engrg, 49, pp. 55–70, 1985.

Tiago CM. *Meshless methods: Extending the linear formulation and its generalization to geometrically exact structural analysis.* Ph.D. Thesis. Instituto Superior Técnico da Universidade Técnica de Lisboa. Lisboa, 2007.

Tiago CM and Pimenta PM. *An EFG method for the nonlinear analysis of plates undergoing arbitrarily large deformations*. Engineering Analysis With Boundary Elements, 32(6), 494-511, 2008.

Tiago CM and Pimenta PM. *Geometrically exact analysis of space frames by a meshless method.* Proceedings of the ECCOMAS Thematic Conference on Meshless Methods, Lisbon, Portugal, July 2005.